**Proceedings of ASME Turbo Expo 2011**
**GT2011**
**June 6-10, 2011, Vancouver, British Columbia, Canada**

# GT2011-46261

# HIGHLY LOADED LPC BLADE AND NON AXISYMMETRIC HUB PROFILING OPTIMIZATION FOR ENHANCED EFFICIENCY AND STABILITY

**I. Lepot** [*], **T. Mengistu** [*], **S. Hiernaux** [†] **and O. De Vriendt** [†]
[*] Cenaero
Rue des Frères Wright 29, B-6041 Gosselies, Belgium
[†] Techspace Aero
Route de Liers, 121, B-4041 Milmort, Belgium

## ABSTRACT

*The present contribution fits into the frame of the ongoing 7th Framework European Project DREAM (valiDation of Radical Engine Architecture systeMs). One of its main themes targets the development of contra-rotating open rotors with variable pitch blades which are known to provide 10 to 15% fuel burn reduction but are noisier than high by-pass turbofans. More specifically, the present research was conducted in the frame of work package 3.4 lead by Techspace Aero, dedicated for one part to the design of a high speed booster adapted to open rotor configurations, and for the second part, from which this paper is issued, to the investigation of 3D geometries to improve LPC efficiency.*

*A reference rotor blade has first been designed, with high loading, especially at hub. To improve its efficiency, a backward sweep has then been applied as it tends to unload midspan sections. However, this performance gain came at the price of severe stall margin degradation, the criticality of the hub region being increased. Based on 1.5 stage 3D RANS simulations, automated surrogate-assisted optimization has then been exploited to respectively evaluate the potential benefit of tailored 2D contouring and 3D hub profiling a posteriori applied to the swept rotor blade and of joint 3D hub profiling and sweep optimization of the unswept baseline rotor blade.*

*The potential benefit of 3D profiling will be demonstrated while the joint 3D profiling and blade stacking optimization shed light on the achievable interesting 3D effects combinations.*

[*]Address all correspondence to this author.

## NOMENCLATURE

ANOVA Analysis of Variance
c chord
DoE Design of Experiments
$D_{Lieb}$ Lieblein diffusion factor
EA Evolutionary Algorithm
H Specific enthalpy
h Blade height
(L)CVT (Latinized) Centroidal Voronoï Tessellations
L/TE Leading/Trailing Edge
LHS Latin Hypercube Sampling
LOO Leave-One-Out
LPC Low Pressure Compressor
$\eta$ Isentropic efficiency
PR Total-to-total Pressure Ratio
P/SS Pressure/Suction Side
$\psi$ Loading factor
R Radius
RBF Radial Basis Functions
s Pitch
SBO Surrogate-Based Optimization
U Mean driving speed

## INTRODUCTION

Increased economical and environmental constraints are currently driving the turbofan evolutions. In order to reduce SFC of next generation turbofans, emphasis is put on higher component efficiency. On the other hand, the necessity to keep the mass and length of the low pressure compressor in an affordable range leads to an increase of the average stage loading $\psi = \frac{\Delta H}{U^2}$. The challenge in LPC blade design hence lies in a difficult compromise between efficiency and stability, which becomes even more stringent as the loading increases. The present work, performed within WP 3.4 of the 7th Framework European Project DREAM, shows how two 3D design approaches, blade sweep and non axisymmetric hub profiling, can be successfully combined in order to improve compressor efficiency without jeopardizing its stability.

The reference compressor stage has been designed by scaling down an existing highly loaded booster front stage (see Fig. 1, displaying the throughflow view). Stage characteristics are given in Table 1 below. One of the main features of the rotor blade is a highly loaded hub section ($\psi = \frac{\Delta H}{U^2} = 0.86$) leading to high diffusion ($D_{Lieb} = 0.46$ at design point) and a shock on the blade suction side due to the high turning of hub sections.

| | |
|---|---|
| Standard mass flow: | 10.1 kg/s |
| Rotor relative inlet Mach: | 0.77 |
| Reynolds number: | 420,000 |
| Rotor standard tip speed: | 220 m/s |
| Relative pitch ($\frac{s}{c}$): | 0.62 (hub) to 0.79 (tip) |
| Rotor blade count: | 76 |
| Blade aspect ratio ($\frac{h}{c}$): | 1.66 |
| Blade hub to tip ratio ($\frac{R_{hub}}{R_{tip}}$): | 0.82 |

**TABLE 1**. TEST CASE CHARACTERISTICS

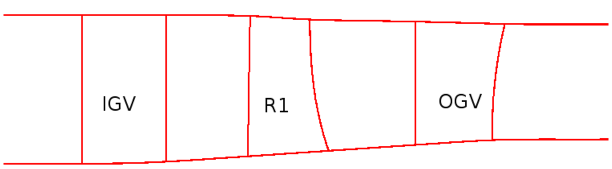


**FIGURE 1**. THROUGHFLOW VIEW

To improve rotor efficiency, a backward sweep has been applied as it tends to unload midspan sections, hence increasing the global mass-averaged efficiency as more flow is passing over midspan sections than near wall sections. However, this 3D effect also increases loading at hub, which could already be considered as critical in the reference design. This induced an earlier corner stall than for the reference unswept blade and a drastically lower stability margin as can be noted from Figure 10.

A classical trend in current compressor designs to cope with diffusion on blade hubs is to use an axisymmetric contouring of the hub surface (see e.g. Refs. [Hoeger et al. 2002], [Speer and Biederman 1995], [Stringham et al. 1998]). This kind of wall profiling can be used to carefully control the diffusion over hub profiles and decrease velocities around the blade by locally increasing the passage area. However, with highly loaded hub designs, the flow structure is mainly driven by stronger cross-flows between blade pressure side and adjacent blade suction side. As this feature is essentially non-axisymmetric, the objective of the present study was to investigate the potential benefit of 3D endwall profiling and assess to what extent a particular design of non axisymmetric hub can reduce the strength of the compressor row secondary flow loss core in order to cope with the high hub loading. Studies of this nature are indeed still quite scarce in the literature.

In Ref. [Harvey 2008] for example, the experiments performed on a linear compressor stator cascade at Cambridge University, showed that the imposed 3D profiling lead to improvement in the exit flow field in terms of local flow reductions in the loss and under-turning in the secondary flow region. The subsequent CFD analysis were then shown to achieve good agreement with the measurements at the design conditions and a reasonable qualitative match at off-design. Information about the reference design methodology can be found in Refs. [Rose et al. 2001,Harvey et al. 2002]. The work presented in Ref. [Harvey 2008] was pursued in Ref. [Harvey and Offord 2008] with a computational study of applying profiled endwalls to a multi-stage HP compressor. The latter study showed that non axisymmetric endwall profiling could be exploited to suppress stator hub corner stall as effectively as 3D blading. How to combine non axisymmetric endwalls with 3D airfoil shaping for LP compressors remained an open question.

In Ref. [Nagel and Baier 2003] both the blade shape and the endwall of a symmetric turbine vane optimizations were conjointly tackled, while Ref. [Germain et al. 2008] combined an extended wall parameterization with the fillet radii on a turbine stage configuration. Back to HP compressors, Ref. [Dorfner et al. 2003] showed to increase the isentropic efficiency by about 1% with 30 parameters that described the hub endwall. For a modern multi-stage LPC with state-of-the-art blading at its design point, the secondary flows and their associated losses are relatively small and largely confined to the endwall regions. Ref. [Muller et al. 2002] showed that endwall modifications in the shape of a bulb or fillet that match the order of magnitude of the incoming boundary layer may help to lower secondary losses. With the stall margin degradation faced here by applying backward sweep to the baseline geometry, it was then decided to further investigate if a modern LP multi-stage compressor could be significantly improved by the retrospective exploitation of non axisymmetric profiling.

Two operating points have been chosen, the design point and a second point closer to the stall region (stall point). The objective is to improve operability and/or efficiency, e.g. by maximizing isentropic efficiency at design point while preserving the stability of the compressor, under a series of mass flow and stage outlet angle constraints. Based on 1.5 stage 3D RANS simulations, automated surrogate-assisted optimization has been exploited to respectively evaluate, in a step by step approach, the potential impact of tailored 2D contouring and of 3D hub profiling applied to the backward swept rotor blade and finally conjoint 3D hub profiling and sweep optimization of the unswept reference rotor blade has been performed.

The paper is structured as follows. The computational chain setup and optimization methodology are first described. After a recall of the optimization specifications and the definition of the backward swept reference geometry, the optimization results are then presented in the order adopted for the study, with successively a posteriori 2D contouring and 3D profiling applied to this backward swept blade. Conjoint 3D profiling and stacking optimization results of the unswept baseline geometry are then presented. These optimization results and flow features of the optimized geometries are analyzed and compared at both design and stall points. 3D surface shapes will be examined in the light of quantitative variance analysis results based upon the exploitation of the surrogate models. Finally, some conclusions and perspectives are drawn.

## DESIGN CHAIN SETUP

### Parameterization

Both CATIA v5 and an in-house blade shape modeler have been coupled and integrated into the design loop, for the 3D profiling of the rotor hub endwall and its stacking modifications respectively. The CAPRI [Haimes and Follen 1998] CAD integration middleware has been exploited in order to provide direct CAD access without manual interventions in the CAD system during the optimization loops. Based on CAPRI, an object-oriented framework has been developed to: a) interact with the underlying CAD system transparently, b) modify the shape design variables, c) regenerate the CAD model and d) provide an updated native geometry representation to be used for the analyses. More information can be found e.g. in Ref. [Iliopoulou et al. 2006]. In the present work, the hub endwall is parameterized under CATIA v5 using a series of B-spline curves and holds 17 parameters in all. Respectively 6 parameters axially, 6 ones radially, and 4 ones azimuthally permit to adjust the surface while an additional parameter allows to apply the 3D profiling up to 3.5% hub axial chord upstream the LE. The locations of the B-spline control points have been chosen so as to provide surface flexibility, surface periodicity in the azimuthal direction, surface continuity, and surface slope continuity.

For the 2D contouring, this non axisymmetric parameterization has been used as a basis and simplified so as to keep an identical framework for the sake of comparison. It holds four parameters, two axial and two radial ones plus a fifth parameter allowing hub contour modification upstream the LE. Radial bumps and material removal are allowed up values amouting to 20% pitch. Finally, regarding the stacking modifications, 2 degrees of freedom have been added as a section, comprised between 30% and 70% span, is allowed to move axially by 20% hub axial chord, whether upstream or downstream.

### Flow Field Evaluation

For all simulations presented hereafter, the multi-block cell-centered elsA code (ensemble logiciel de simulation en Aerodynamique [Plot et al. 2002]) developed at ONERA, has been employed while for the mesh generation the AutoGrid software (Numeca International) has been used.

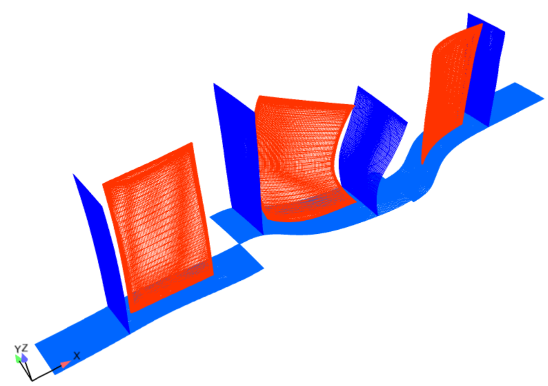

**FIGURE 2**. 1.5 STAGE RANS SIMULATIONS SETUP (POST-TREATMENT PLANES IN BLUE)

One and half stage simulations have been integrated into the design loop, considering both upstream and downstream stators of the parameterized rotor blade, as illustrated in Figure 2. The post-treatment planes considered for performance evaluation are highlighted in blue. RANS simulations with $k-\varepsilon$ two-additional equations turbulence model have been conducted, without wall functions. To define the number of grid points of the reference geometry mesh, a mesh dependence study has been performed. The overall mesh size is about 3.6 million points: 1.4 million points for the rotor blade, including tip gap modeling and about 1.1 million cells per stator, preserving a y+ value below 1 along blades and endwalls. For the near stall point, the outlet mass flow is imposed while a throttle condition (imposed outlet pressure over mass flow) is used at design point.

As far as pseudo-time integration is concerned, convergence to steady state is accelerated thanks to a 2 level multigrid V-cycling, which leads to a run time of about 3 hours on 60 64-bit Xeon computation cores of Cenaero's Linux cluster.

## Optimization Platform

An adequate and general answer to optimization based on long running and computationally intensive analysis lies in the exploitation of surrogate models. Recent advances in Surrogate-Based Optimization (SBO) indeed bring the promise of efficient global optimization to reality. SBO uses most of the time surrogates or approximations in lieu of the expensive analysis results to contain the computational time within affordable limits (see e.g. Refs [Jones et al. 1998], [Queipo et al. 2005] and [Forrester and Keane 2009]), with occasional recourse to the high-fidelity model. Since the computationally affordable design selections made to produce the initial set of data supporting the surrogates construction will almost inevitably miss certain features of the landscape, the construction of trustable surrogates often requires further, judiciously selected calls to the analysis codes, in a so-called online framework. These additional calls, or infill points, are typically selected either in areas where the surrogates are thought to be inaccurate or, alternatively, where the surrogate models suggest that particularly interesting combination of variables lies, aiming for the Graal quest of optimum balance between exploration and exploitation.

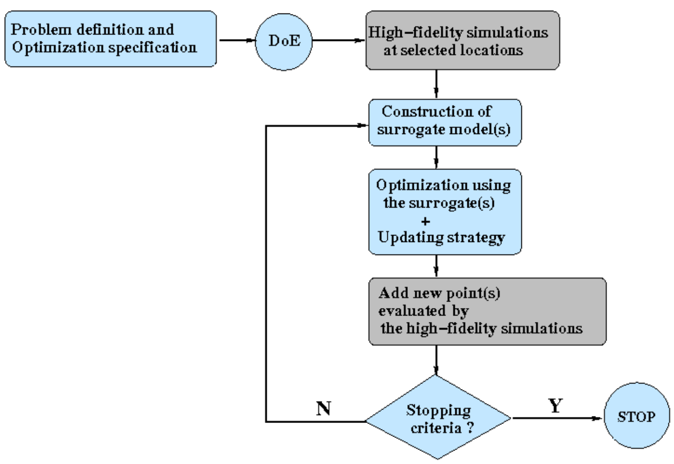


**FIGURE 3**. ONLINE SURROGATE-BASED OPTIMIZATION FRAMEWORK

Cenaero's in-house optimization platform Minamo has been exploited in the present work. Minamo implements mono- and multi-objective Evolutionary Algorithms (EAs) efficiently coupled to surrogate models. Such methods are stochastic, population-based search techniques and widely used as efficient global optimizers as such zero-order optimization techniques are indeed robust and able to cope with noisy, discontinuous, non-differentiable, highly non-linear and uncomputable functions. Most importantly, they also permit to simultaneously handle multiple physics as well as large numbers of design variables and multiple objectives.

Figure 3 recalls the major steps of an SBO online design cycle. A crude initial database is built by choosing a set of points in the design space and conducting high-fidelity simulations at the selected sample points. Based on this DoE exercise, surrogate models are constructed in order to build an analytical relationship between the design parameters and the expensive simulation responses, objectives and constraints. Besides classical filling techniques such as quasi-random sequences and Latin Hypercube Samplings, Minamo features a priori sampling techniques based on Centroidal Voronoï Tessellations (CVT) and Latinized Centroidal Voronoï Tessellations (LCVT) [Saka et al. 2007], typically offering lower discrepancy than pure CVT and higher volumetric uniformity than pure LHS and exploited in the present work. In terms of generic interpolation models, Minamo features Radial Basis Functions (RBF) networks, ordinary and universal Kriging. In the training process, a trade-off must be determined between the accuracy of the surrogate and its computational cost. For the RBF network exploited in the present work, the surrogate models are generated without the user's prescription of the type of basis function and hyperparameter values. The implementation autonomously chooses the type of basis functions (Multiquadrics or Gaussian) and adjusts the width parameter of each basis function in order to obtain an accurate surrogate model, the adjustment being essentially built on the cost-effective Leave-One-Out [Meckesheimer et al. 2002] (LOO) procedure proposed by Rippa [Rippa 1999]. An efficient framework for managing global and local surrogate models is used, based on the move-limit procedure [Torczon and Trosset 1998].

Furthermore, Minamo offers an efficient handling of simulation failures. Indeed, when optimization is carried out using high-fidelity numerical simulations, it is an inevitable fact that not all simulations provide reliable results (due to an inappropriate mesh, failed geometry regeneration, etc.). The best practice is to try to make the simulation chain as robust as possible, and let the optimizer take care of the simulation failures. With Minamo, two families of surrogate models are managed simultaneously, namely the response models and the failure prediction models. The idea is to bias the search away from failed sample points by penalizing, via adequate constraints, regions containing simulation failures.

# OPTIMIZATION RESULTS

## Optimization Specifications

Two operating points are considered, the design point and a second point close to numerical stall (which will be called "stall" for simplification reasons). For the 2D and 3D profiling optimizations, applied a posteriori to the backward swept reference blade, the objective was to maximize the total-to-total pressure ratio at stall (post-treatment planes upstream the first stator and downstream the second stator) while preserving rotor isentropic efficiency at design point (see upstream and downstream post-treatment planes set around the rotor in Fig. 2). For the conjoint 3D profiling and stacking optimization, departing from an unswept reference blade, the objective was to maximize rotor isentropic efficiency at design point while preserving the total-to-total pressure ratio at stall.

The exit flow angle at the outlet, in the post-treatment plane downstream the second stator, was constrained so that the local values at 10%, 20%, 40%, 60%, 80% and 90% span were imposed to be inferior to the values of the reference geometry. The total-to-total pressure ratio and mass flow rate at design point were imposed to remain above their reference value, while the mass flow rate at stall point was fixed. Finally, to preserve stability, the ratio between total-to-total pressure ratio at stall and total-to-total pressure ratio at design was also constrained to remain above the reference value.

### Swept Reference Definition

A reference rotor blade has first been designed, with high loading, especially at hub. To improve its efficiency, a backward sweep (see e.g. Refs. [Denton and Xu 2002, Passrucker et al. 2003]) has then been applied as it tends to unload midspan sections, hence increasing the global mass-averaged efficiency as more flow is passing over midspan sections than near wall sections. However, this 3D effect also increased loading at hub, which could already be considered as critical in the baseline design. This lead to an earlier corner stall than for the reference blade and a drastically lower stability margin. Figure 4 presents selected (manually) tested backward sweeps and their effect on stability and efficiency, which clearly shows that the gain in efficiency is only obtained at the price of degradation in terms of operability.

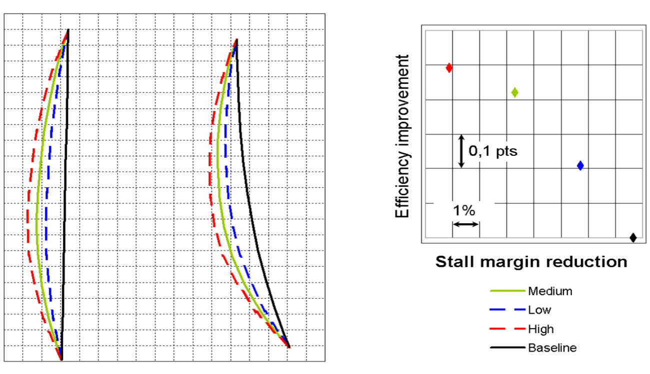


**FIGURE 4**. TESTED SWEEPS AND EFFECTS ON STALL MARGIN AND EFFICIENCY

The geometry labelled "Medium" in Figure 4 has been chosen by Techspace Aero as reference swept blade for the subsequent studies. Figure 5(b) clearly shows an increased load at the leading edge of the hub sections and an unloading of midspan sections at the leading edge. This results in a decreasing of diffusion factor, and hence of losses at midspan that can be seen on Figure 5(a).

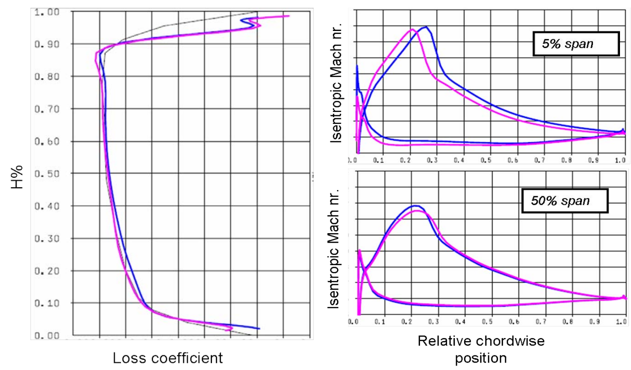


(a) Loss distribution on baseline (blue) and backward swept (Medium - pink) blades

(b) Isentropic Mach distribution on baseline (blue) and backward swept (Medium - pink) blades

**FIGURE 5**. EFFECT OF SWEEP ON ISENTROPIC MACH DISTRIBUTION AND LOSSES

### 2D and 3D Profiling

For the first studies conducted, applying a posteriori profiling without altering the blade, the backward swept blade described here above has been considered as reference. The primary objective of the study was hence to compare how 2D and 3D profiling could respectively compensate for the degraded stall margin while preserving efficiency at design point. As has been underlined in the Section describing the parameterization, a 2D parameterization, with 2 axial and 2 radial degrees of freedom was derived as a subset of the flexible 3D hub parameterization so as to obtain comparable results. In addition, again similarly to the 3D profiling, an additional degree of freedom allowed contour modification up to 3.5% hub axial chord upstream the rotor LE.

Starting with the 2D contouring, a first database comprising a little less than 50 samples, i.e. 10 times the number of parameters was generated. This lead to excellent LOO cross-correlation coefficients for the global surrogates, e.g. above 0.9 for the isentropic efficiency at design point. The optimization was then carried out and clearly showed a stabilized trend towards a marked hollow from 60% to 90% hub axial chord. However, the indced flow modifications did not compensate for the stall margin degradation although the global and local surrogate models appeared very reliable.

Another 60 samples, now allowing for variations of the 17 3D hub endwall parameters, were then added to the database. Although the LOO cross-correlation coefficients were indicative of the much higher non linearities to be captured (e.g. with a LOO cross-correlation coefficient dropping to 0.55 for isentropic efficiency at design point), the optimization proved able to obtain a stabilized 3D endwall shape attaining the goal of compensating the stall margin degradation while preserving isentropic efficiency at design point as illustrated in Figure 10. To draw the performance map, the numerical stall point was defined as the last stable, low mass flow point at which the conservativity default (relative difference between inlet and outlet mass flow) remains steadily below 0.05% for the last 300 pseudo-time iterates.

It may be noted that for the periodic retraining of the surrogates along the design, ensuring that the surrogate models become more and more representative of the evolving search regions, systematically the optimized geometry suggested by the optimization and an additional sample, minimizing an error estimator based upon LOO cross-validation, were evaluated with high-fidelity CFD and fed back into the database at each design iteration.

Figure 6 displays the contour levels of the optimized 3D profiling in terms of radius delta with respect to the axisymmetric vein, non dimensionalized with respect to the pitch. One can clearly note an important bump in the rear part of the suction side, and conversely, a marked digging along suction side beyond 60% hub axial chord. This pattern, contrary to classical 3D profiling aiming at reducing secondary flows by diminishing the blade-to-blade pressure gradient, enhances the cross flow precisely at the axial location at which corner stall starts for the reference configuration, both at design and stall points. As a consequence, one could interpret this locally enhanced cross-flow as a way to energize the boundary layer and postpone the corner stall development.

Figure 7 illustrates the oil traces and total pressure on the suction side at design point for the backward swept axisymmetric reference and for the optimized 3D hub profiling respectively. In the same fashion, Figure 8 displays the oil traces and total pressure on the hub endwall at stall point. The augmented cross-flow and the impact on the corner stall is clearly visible.

Table 2 summarizes the 1st order Sobol indices obtained following quantitative variance analysis [Saltelli et al. 2000, Sobol 1993, Saltelli 2002] of the surrogates. On the one hand, one can clearly note that the most influential parameters appear similar for design and stall points. This is fully in line with the impact of the 3D profiling, energizing the boundary layer where the corner stall originates, whether design or stall point is considered. On the other hand, the levers driving isentropic efficiency and total-to-total pressure ratio also show to be distinct, as could be expected. Overall, the elevation amplitudes constitute the key parameters, while the important volume of higher order interaction terms essentially consists in axial positioning and radius cross-

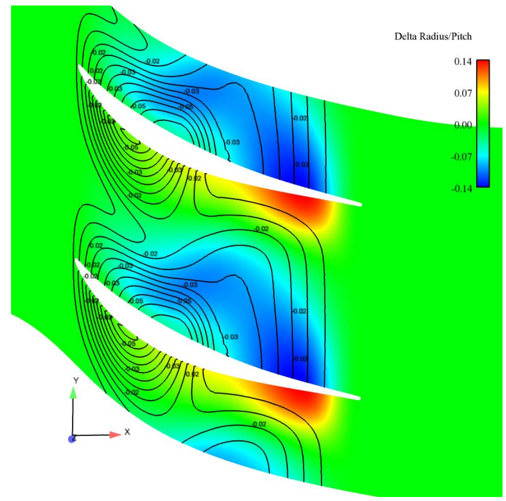


**FIGURE 6**. 3D PROFILING ELEVATION CONTOURS A POSTERIORI APPLIED TO THE BACKWARD SWEPT REFERENCE

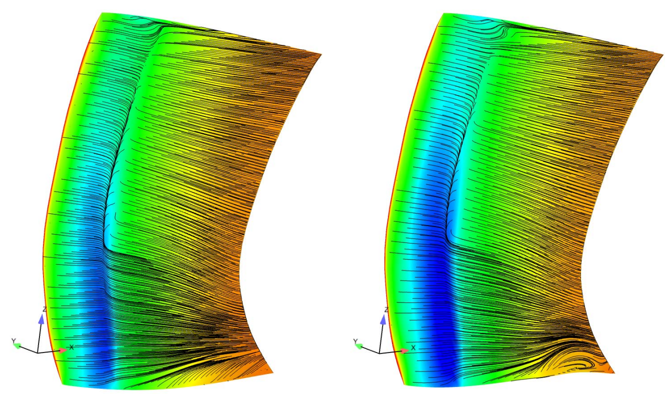

(a) Backward swept axisymmetric reference (b) Backward swept blade with optimized 3D profiling

**FIGURE 7**. SUCTION SIDE OIL TRACES AND TOTAL PRESSURE AT DESIGN POINT

terms a shown by a second-order ANOVA. The main levers for isentropic efficiency appear to be, in terms of first order indices, located near the SS and in the aft part of the blade passage, which again underlines that the 3D profiling impact targets the corner stall. Regarding total-to-total pressure ratio, the most influential parameters are the elevation amplitudes driving the sections opening, at midpitch and near the rear part of the pressure side.

Figures 11 display the total pressure profiles along the span at the exit of the rotor (left) and downstream stator (right) at design point for each studied configuration. The effect of 3D profiling at hub is clearly indicated by an increase of pressure at hub, compared to baseline and reference swept blades. This

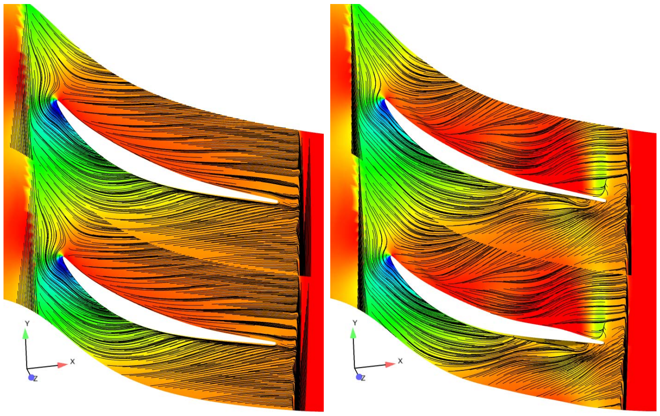

(a) Backward swept axisymmetric reference (b) Backward swept blade with optimized 3D profiling

**FIGURE 8**. HUB OIL TRACES AND TOTAL PRESSURE AT STALL POINT

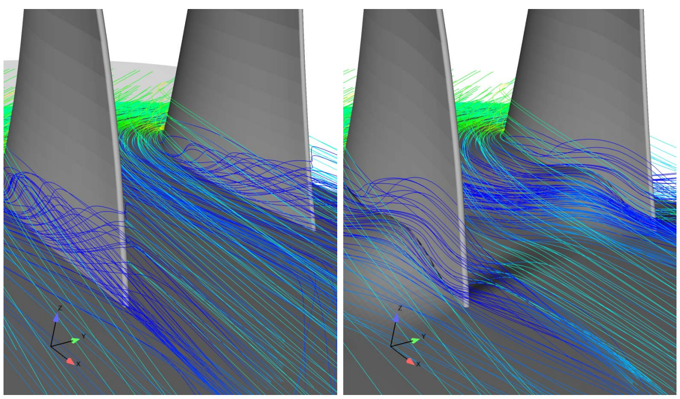

(a) Backward swept axisymmetric reference (b) Backward swept blade with optimized 3D profiling

**FIGURE 9**. HUB CORNER STALL - STREAMLINES AT STALL POINT

increase of pressure is still present after the outlet stator. Figures 12 then display the total pressure profiles along the span at the exit of the rotor (left) and downstream stator (right) at stall point. One can notice that at this point, the pressure profile is constant along height for both unswept baseline and reference swept blades from hub up to 20% span. This denotes a flow separation at hub that induces flow deviation and limits the compression capacity of the blade hub sections and finally leads to stall. The hub-profiled blades, on the contrary, still present at hub a good compression capacity, and increased stall margin.

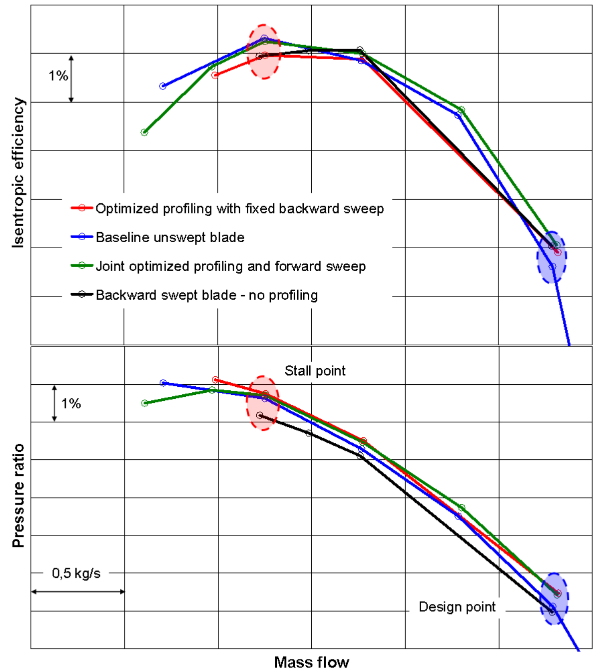


**FIGURE 10**. STAGE PERFORMANCE MAP

| | Design point | | Stall point | |
|---|---|---|---|---|
| Parameters | $\eta$ | PR | $\eta$ | PR |
| P1 | 0.48% | 0.54% | 0.48% | 0.38% |
| P2 | 17.97% | 3.58% | 39.55% | 19.02% |
| P3 | 2.35% | 3.57% | 0.11% | 2.79% |
| P4 | 6.73% | 0.77% | 5.43% | 5.40% |
| P5 | 0.76% | 0.27% | 0.24% | 0.10% |
| P6 | 0.65% | 4.35% | 0.17% | 4.87% |
| P7 | 2.29% | 0.64% | 2.63% | 0.86% |
| P8 | 1.23% | 9.66% | 0.25% | 5.00% |
| P9 | 0.20% | 0.43% | 1.11% | 1.74% |
| P10 | 1.29% | 2.11% | 0.73% | 1.26% |
| P11 | 0.71% | 0.78% | 0.12% | 0.01% |
| P12 | 3.04% | 34.52% | 0.73% | 22.21% |
| P13 | 5.28% | 2.08% | 5.59% | 3.11% |
| P14 | 0.35% | 0.43% | 1.29% | 0.22% |
| P15 | 14.30% | 1.95% | 4.47% | 0.41% |
| P16 | 1.41% | 0.17% | 2.57% | 0.57% |
| P17 | 0.06% | 0.16% | 1.07% | 0.49% |
| Higher order | 40.90% | 33.98% | 33.47% | 31.58% |

**TABLE 2**. ANALYSIS OF VARIANCE (1ST ORDER INDICES)

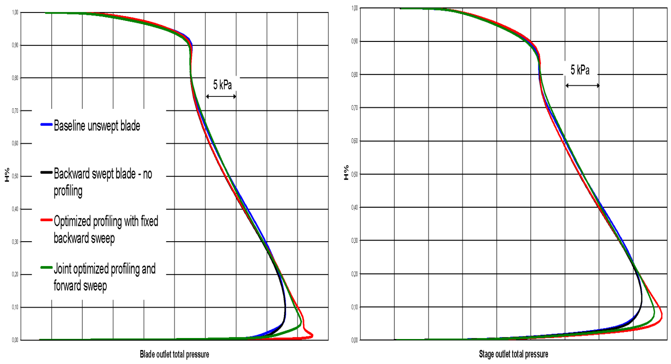


(a) Rotor exit (b) Stage exit

**FIGURE 11**. TOTAL PRESSURE AT ROTOR AND STAGE EXIT - DESIGN POINT

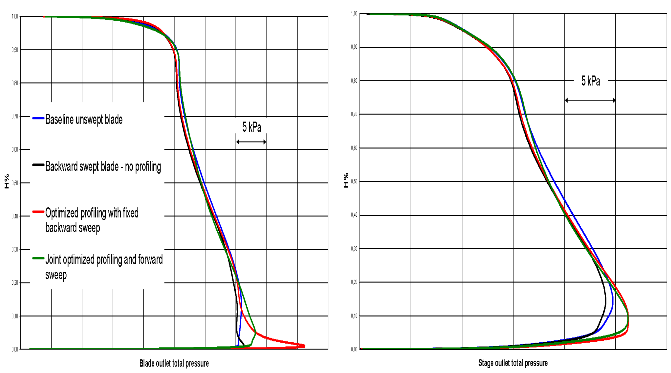


(a) Rotor exit (b) Stage exit

**FIGURE 12**. TOTAL PRESSURE AT ROTOR AND STAGE EXIT - STALL POINT

## Conjoint 3D Profiling and Stacking Optimization

Finally, simultaneous 3D endwall and stacking optimization was carried out with 17 parameters for the 3D hub and 2 additional parameters for the stacking. An initial database of about 120 parameteric combinations (i.e. about 6 times the number of parameters) was generated, leading to acceptable initial LOO cross-correlation coefficients, e.g. in the order of 0.6 for isentropic efficiency at design point, main objective of this last optimization. After 15 to 20 design iterates, the interesting geometries identified did present backward sweep and a 3D hub profiling similar to the results obtained previously with a posteriori profiling. However, after 40 to 45 iterates, the optimization finally stabilized in a quite different region of the conception space, even more interesting in terms of isentropic efficiency, with a forward swept blade accompanied by a much shallower profiling: a slight depression on the suction side of the blade, near the leading edge and a slight depression on the pressure side at midchord (see Fig. 13). This could be interpreted as a skewed version of the near leading edge hollow that would typically result from 2D contouring focusing on isentropic efficiency raise through reduced suction side peak isentropic Mach number. The decrease and smoothing of the suction side isentropic Mach number is indeed clearly visible in Figures 14, displaying oil traces and pressure contours on the suction side for the unswept reference blade and optimized forward swept configuration respectively, and in Figure 15, showing the static pressure evolution around the blade at 15% span. The selected forward swept optimized configuration was also recomputed with axisymmetric hub. Interestingly, the superposition of static pressure distributions in Figure 15 then shows that regardless of the 3D profiling shallowness, it is this profiling applied to the forward swept blade that helps reducing the suction side shock up to 25% of the blade span.

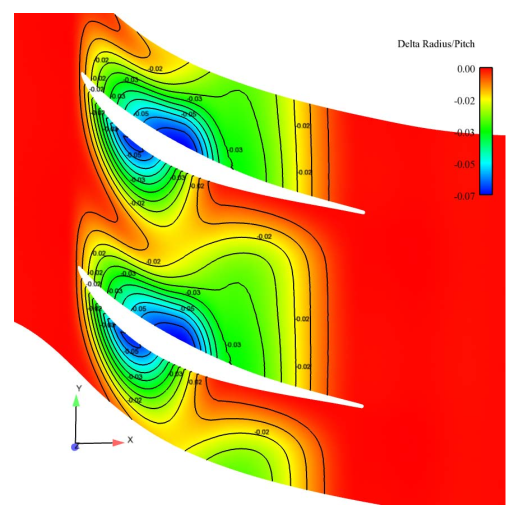


**FIGURE 13**. OPTIMIZED 3D PROFILING ELEVATION CONTOURS ASSOCIATED WITH A FORWARD SWEPT BLADE

Table 3 details the first order Sobol indices obtained following quantitative variance analysis of the surrogates. The parameters labelled S1 and S2 denote the additional stacking degrees of freedom allowed. ¿From these first order indices, one can note that the stacking, speaking in relative terms, provides more leverage for improving stability with respect to performance gain. This appears logical in regard with the final stabilized optimized shape, which features forward blade sweep and tailored 3D hub, highlighting the hub critical nature of the unswept baseline already. The elevation amplitude close to the suction side leading edge, characterized by parameter P2, appears as the most influ-

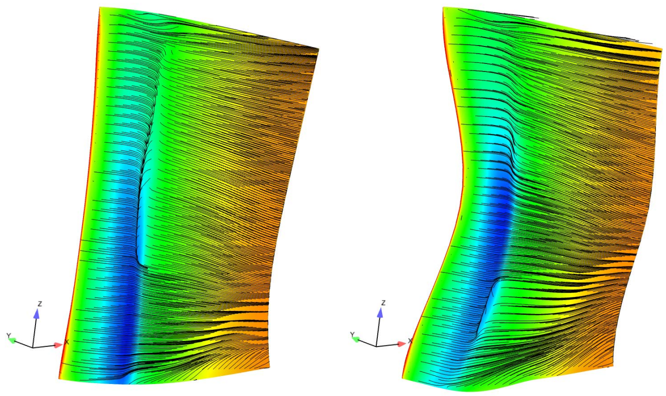

(a) Unswept axisymmetric reference (b) Optimized forward swept blade with 3D profiling

**FIGURE 14**. SUCTION SIDE OIL TRACES AND TOTAL PRESSURE AT DESIGN POINT

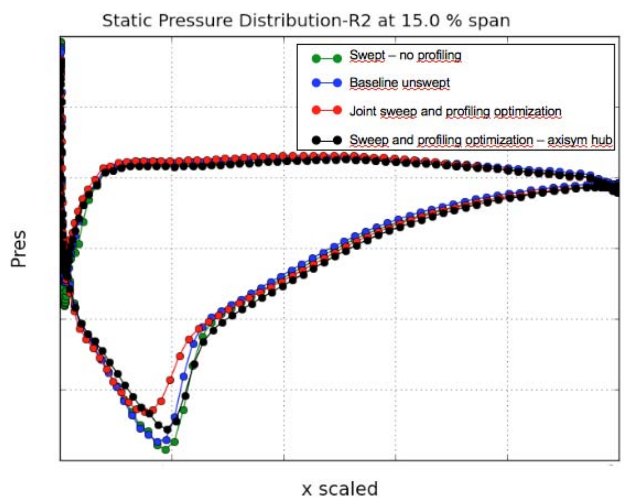


**FIGURE 15**. STATIC PRESSURE DISTRIBUTION AT 15% SPAN

ential parameter at stall point, and logically for both isentropic efficiency and total-to-total pressure ratio.

Regarding desing point, leverage in terms of total-to-total pressure ratio but now also in terms of isentropic effiency is obtained through the elevation amplitude P12, essentially driving the section opening at midpitch. This appears logical since by applying forward sweeping, the loading of the midspan sections is increased and the parameters allowing for section opening may gain more influence as they can help reducing the shock losses.

| | Design point | | Stall point | |
|---|---|---|---|---|
| Parameters | $\eta$ | PR | $\eta$ | PR |
| P1 | 1.49% | 0.66% | 0.80% | 0.68% |
| P2 | 3.48% | 3.59% | 49.36% | 35.20% |
| P3 | 0.28% | 0.13% | 0.22% | 0.12% |
| P4 | 5.53% | 0.99% | 5.06% | 3.72% |
| P5 | 0.99% | 0.86% | 0.22% | 0.29% |
| P6 | 2.96% | 1.14% | 1.63% | 0.33% |
| P7 | 1.47% | 0.54% | 0.24% | 0.18% |
| P8 | 0.07% | 7.44% | 0.77% | 2.34% |
| P9 | 0.44% | 0.19% | 0.04% | 0.16% |
| P10 | 0.40% | 0.36% | 1.02% | 1.43% |
| P11 | 0.51% | 0.68% | 0.01% | 0.06% |
| P12 | 12.47% | 32.38% | 1.54% | 10.49% |
| P13 | 1.06% | 0.78% | 2.17% | 2.42% |
| P14 | 1.93% | 1.05% | 0.54% | 0.66% |
| P15 | 8.66% | 12.98% | 4.55% | 4.22% |
| P16 | 0.31% | 0.23% | 0.68% | 0.49% |
| P17 | 0.08% | 0.32% | 0.32% | 0.57% |
| S1 | 1.32% | 0.91% | 0.08% | 0.10% |
| S2 | 3.59% | 6.38% | 5.18% | 11.32% |
| Higher order | 52.96% | 28.38% | 25.57% | 25.22% |

**TABLE 3**. ANALYSIS OF VARIANCE (1ST ORDER INDICES)

## CONCLUSIONS

A reference LPC highly-loaded rotor blade has first been designed and a backward sweep has been applied to this baseline to improve efficiency by unloading the midspan sections. This sweep however increased the cross-flow at hub sections leading to earlier stall. Based on 1.5 stage 3D RANS simulations, an automated surrogate-assisted optimization loop has been set up and exploited to respectively evaluate, in a step by step approach, the potential impact of tailored 2D contouring and of 3D hub profiling applied to the backward swept rotor blade and finally conjoint 3D hub profiling and sweep optimization of the unswept reference rotor blade has been performed.

While a classical 2D contouring could not compensate for the stability loss coming as the price of the efficiency gain with the backward sweeping of the reference blade, the non axisymmetric hub profiling revealed able to modify the secondary flows at hub and reestablish an acceptable stability range while preserving the efficiency gain of the backward swept blade.

Thanks to the global exploration capabilities of the surrogate-based automated design loop set up, the joint 3D profiling and axial blade stacking optimization then further shed light on the achievable promising 3D effects combinations, pointing out backward sweep with adequate profiling following the first design iterates while the optimization finally stabilized in a different region of the conception space, with a forward swept rotor blade and a different tailored 3D hub. Schematically, while in the first (backward swept) configuration, the sweeping improves efficiency at design point while the non axisymmetric hub compensates for stability; in the second (forward swept) configuration, conversely, the sweeping targets the critical hub loading and improves operability while the 3D profiling locally opens up the section in order to reduce the shock losses.

Following study of the dynamical behaviour of both configurations at high speed, Techspace Aero selected the backward swept configuration with associated 3D profiling to be tested at the Von Karman Institute within the FP7 DREAM project, in order to experimentally verify the results of the present study, focused on understanding the joint aerodynamic impact of sweeping and 3D profiling. The fact that the geometry that gives the best performance improvement could not be retained due to dynamic behaviour issues highlights the fact that multi-disciplinary optimization is mandatory to further jointly optimize blades and endwalls, the associated increased run time and computational budget being worth the investment.

## ACKNOWLEDGMENT

The work presented here was carried out in the frame of the DREAM Project with co-funding from the European Commission within the 7th Framework Program. The support of the European Commission and of the DREAM WP 3.4 partners is gratefully acknowledged.

## REFERENCES

[Hoeger et al. 2002] Hoeger, M., Cardamone, P.,Fottner, L., *Influence of endwall contouring on the transsonic flow in a compressor blade*, ASME paper GT-2002-30440 in *Proceedings of ASME TurboExpo 2002*, Amsterdam, The Netherlands, June 2002.

[Speer and Biederman 1995] Speer, P.A., Biederman, B.P., *Flow directing assembly for the compression section of a rotary machine*, US Patent nr. 5397215, March 1995.

[Stringham et al. 1998] Stringham, G.D., Cassen, B.N., Prince, T.C., Yeung, P.F., *Design and development of a nine stage axial flow compressor for industrial gas turbines*, in *Proceedings of the 1998 International Gas Turbine & Aeroengine Congress & exhibition*, Stockholm, Sweden, June 1998.

[Harvey 2008] Harvey, N., W., 2008, *Some effects of non-axisymmetric end wall profiling on axial flow compressor aerodynamics. Part I: Linear cascade investigation*, ASME Paper GT2008-50990.

[Rose et al. 2001] Rose, M., G., Harvey, N., W., Seaman, P., Newman, D., A. and McManus, D., 2001, *Improving the efficiency of the TRENT 500 HP turbine using non-axisymmetric endwalls. Part II: Experimental validation*, ASME Paper 2001-GT-0505, New Orleans, Louisiana, USA.

[Harvey et al. 2002] Harvey, N., W., Brennan, G., Newman D., A. and Rose, M., G., 2002, *Improving turbine efficiency using non-axisymmetric endwalls: validation in the multi-row environment and with low aspect ratio blading*, ASME Paper GT-2002-30337, Amsterdam, The Netherlands.

[Harvey and Offord 2008] Harvey, N., W. and Offord, T., P., 2008, *Some effects of non-axisymmetric end wall profiling on axial flow compressor aerodynamics. Part II: Multistage HPC CFD Study*, ASME Paper GT2008-50991.

[Nagel and Baier 2003] Nagel, M., G. and Baier, R., D., 2003, *Experimentally verified numerical optimization of a 3D-parameterized turbine vane with non-axisymmetric endwalls*, ASME Paper GT2003-38624, Atlanda, Georgia, USA.

[Germain et al. 2008] Germain, T., Nagel, M., Raab, I., Schuepbach, P., Abhari, R.,S. and Rose, M., 2008, *Improving efficiency of a high work turbine using non-axisymmetric endwalls. Part I: Endwall design and performance*, ASME Paper GT2008-50469.

[Dorfner et al. 2003] Dorfner, C., Eberhard, N. and Voss, C., 2007, *Axis-asymmetric profiled endwall design using multi-objective optimization linked with 3D RANS-flow-simulations*, ASME Paper GT2007-27268, Montreal, Canada.

[Muller et al. 2002] Muller, R., Sauer, H., Vogeler, K. and Hoeger, M., 2002, *Influencing the secondary losses in compressor cascades by a leading edge bulb modification at the endwall*, ASME Paper GT2002-30442, Amsterdam, The Netherlands.

[Haimes and Follen 1998] Haimes, R. and Follen, G., 1998, *Computational Analysis Programming Interface*, International Conference on Numerical Grid Generation in Computational Field Simulations, University of Greenwich, United Kingdom.

[Iliopoulou et al. 2006] Iliopoulou, V., Lepot I. and Geuzaine, P., 2006, *Design optimization of a HP compressor blade and its hub endwall*, ASME Paper GT2008-50293, Berlin, Germany.

[Plot et al. 2002] Plot, S., Billonnet, G. and Castillon, L., 2002, *Turbomachinery Flow Simulations Using elsA Software: Steady Validations and First Abilities for Unsteady Computations*, Proceedings of the 38th AIAA/ASME/SAE/ASEE Joint Propulsion Conference and Exhibit, Indianapolis, USA.

[Jones et al. 1998] Jones, D. R. , Schonlau M., Welch W. J., 1998, *Efficient Global Optimization of Expensive Black-Box Functions*, Journal of Global Optimization, Volume 13, Number 4, Pages 455-492.

[Queipo et al. 2005] Queipo, N. V., Haftka, R. T., Shyy, W., Goel, T., Vaidyanathan R., Tucker P. K., 2005, *Surrogate-based analysis and optimization*, Progress in Aerospace Sciences, Volume 41, Issue 1, Pages 1-28.

[Forrester and Keane 2009] Forrester, A. I. J., Keane, A. J., 2009, *Recent advances in surrogate-based optimization*, Progress in Aerospace Sciences, Volume 45, Issues 1-3, Pages 50-79.

[Saka et al. 2007] Saka Y, Gunzburger M, Burkardt J., 2007 *Latinized, improved LHS, and CVT point sets in hypercubes*, International Journal of Numerical Analysis and Modeling, Volume 4, Number 3-4, Pages 729-743.

[Rippa 1999] Rippa S., 1999, *An algorithm for selecting a good value for the parameter c in radial basis function interpolation*, Advances in Computational Mathematics, Volume 11, Number 2-3, Pages 193-210.

[Meckesheimer et al. 2002] Meckesheimer, M., Booker, A., J., Barton, R., R. and Simpson, T., W., 2002, *Computationally inexpensive meta-model assessment strategies*, *AIAA JOURNAL*, Vol. **40**, No. 10, pp. 2053-2060.

[Torczon and Trosset 1998] Torczon V, Trosset M W, 1998, *Using approximations to accelerate engineering design optimization*, AIAA-98-4800 in the Proceedings of the 7th AIAA/NASA/USAF/ISSMO Symposium on Multidisciplinary Analysis and Optimization.

[Denton and Xu 2002] Denton, J.D., Xu, L., *The effect of lean & sweep on transsonic fan performance*, ASME paper GT-2002-30327 in *Proceedings of ASME TurboExpo 2002*, Amsterdam, The Netherlands, June 2002.

[Passrucker et al. 2003] Passrucker, H., Engber, M., Kablitz, S., Hennecke, K., *The effect of forward sweep in a transsonic compressor rotor* in *Proceedings of the 5th European Turbomachinery Conference*, Praha, Czech Republic, March 2003.

[Saltelli et al. 2000] Saltelli, A., Chan, K. and Scott, E. M., 2000, *Sensitivity analysis*. Wiley.

[Sobol 1993] Sobol, I. M., 1993, *Sensitivity analysis for non-linear mathematical models*, Math. Modelling Comput. Exp., 1, pp. 407414.

[Saltelli 2002] Saltelli, A., 2002, *Making best use of model evaluations to compute sensitivity indices*, Computer Physics Communication, 145, pp. 580297.

 